ISSN: 1343-4292
Volume 140, Issue 01, April, 2022

Structure and magnetic properties of Zn-Mn-Fe_2O_4 prepared by Sol-Gel method

Muthana El ttayef Abbas[1], Zena Mohammed Ali abbas[1*]

Department of physics, University of Diyala, College of Science, Iraq[1]

Corresponding author: 1*

ABSTRACT— In order for the nanomaterials to be utilized, it is vital to be able to control the structural and magnetic properties of the Mn-Zn-ferrites nanocomposite by sol-gel nanocomposite generated by sol – gel method at 650, 750, and 850 ^oC. An examination into the possibility of producing the Mn-Zn-ferrites (NPs) by sol-gel as prospective structure-tunable nanomaterials is described in this report. X-ray diffraction (XRD), field emission-scanning electron microscopy (FE-SEM), Fourier-transform infrared (FTIR) spectroscopy and Vibrating Sample Magnetometer (VSM) analysis were used to characterize the structural and magnetic properties of the Mn-Zn-ferrites by sol-gel. The crystallite sizes range from 15 to 18 nm, and the cubic structure of the ferrites shows up in XRD (NPs). Nanoparticles having a particle size of 27.77 to 72.04 nm were found in the produced Mn-Zn-ferrites. In the case of the Mn-Zn-ferrites, prominent FT-IR absorption peaks at 400 and 500 cm-1 indicated the presence of Fe-O, Mn-O, and Zn-O vibrational bands. Results from the VSM demonstrated that the magnetic nature of materials changed dramatically from pristine as magnetization rose and coercivity decreased with Mn-Zn-ferrites nanoparticles. Finally, an optimal magnetic parameter value (Ms =0.80 emu/g and Hc =75 Oe) at (850) ^oC was obtained from the data.

KEYWORDS: Mn-Zn-ferrites NPs; Nanocomposite; Structural and Magnetic properties; Sol-gel method.

1. INTRODUCTION

In recent years, magnetic oxide nanostructures have piqued the public's curiosity due to their unique properties that set them apart from their bulk counterparts, as well as the wide range of potential applications for which they've been developed. A-B exchanges, B-B exchanges, and A-A exchanges are just some of the many types of superexchange contacts that occur in spinel ferrite, which are mediated by oxygen ions in a face-centered cubic (FCC) lattice. There are cations in the A-site and B-site of spinel ferrites that influence their magnetic characteristics [1- 4]. super exchange interactions may be more powerful when cations are swapped than when they are not.

Particle size and shape, morphology, and chemical composition all play important roles in determining the samples' physical qualities, however these factors cannot always be controlled during the nanoparticle production process [5- 7].

For Manganese-Zinc-Ferrite (Mn-Zn-Fe_2O_4) nanocomposite prepared through ceramic methods like sol-gel, the composition, cationic distribution and thermal behavior of oxygen are very often in-ter related [8], leading to an important dependence of the mi-cross structure and therefore its physical properties, with the atmosphere and heat treatment temperatures [9], [10].

Despite this, sol-gel synthesis is a viable option with significant economic and technological advantages as well as excellent reproducibility, and it can produce monodisperse nanoparticles with good crystallinity

when the synthesis process is conducted with the right control [11- 14]. By using XRD analysis (XRD-6000/Japan), the (Mn-Zn-Fe_2O_4) nanocomposite was characterized and the findings were compared to the JCPDS card data (Joint Committee on Powder Diffraction Standards). In Iraq's Nanotechnology and Advanced Materials/Materials Research Department/Ministry of Science and Technology, XRD measurements have examined the orientation of (Mn-Zn-Fe_2O_4) nanocomposite grown samples. In Iran-Mashhad, "(Tescan Mira3 FE-SEM-Czechia)" employed FE-SEM to analyze the morphology and particle size of (Mn-Zn-Fe_2O_4). Fourier transformed infrared spectrum (FTIR) was utilized to study the functions group and vibrations modes utilizing a potassium bromide (KBr) beam splitter and a mid IR triglycine sulfate (TGC) detector for the polarized IR reflectance. The magnetic characteristics were examined utilizing an MPMS XL, Quantum Design SQUID magnetometer by VSM.

2. Experimental work

2.1 Materials and Methods

The materials used in the preparation of the ferrite compound by sol-gel auto combustion method. Iron (III) nitrate ($Fe(NO_3)_{3.9}H_2O$) salt, Ammonia solution (NH3) (Sigma-Aldrich, India, Purity (97.99%)), Citric acid ($C_6H_8O_7.H_2O$), and from a local market, Sigma-Aldrich, India's $Zn(NO_3)_{2.6}H_2O$ was purchased with a purity of 99.99 % (Baghdad, Iraq). All of the solutions were made with water that had been distilled using a water distiller (Gallenkamp, England). A local market in Baghdad, Iraq, sells manganese (II) nitrate ($Mn(NO_3)_{2.4}H_2O$), sold by Sigma-Aldrich and purified to 99.99% purity).

2.2 Synthesis from the Mn-Zn-ferrites nanocomposite by Sol-Gel method

15 mL of distilled water was used to dissolve the metal nitrate and citric acid. They're all mixed together in a glass beaker to make one final solution, A magnetic stirrer at high speeds is used to completely mix the solution at room temperature until it becomes smooth and slimy red-colored, as illustrated in the image (1a). It was done by dripping ammonia into the mixed solution, which was stirred constantly to keep the pH level stable until it reached (7), as seen in the figure (1 b). To achieve homogeneity, stir the components together for half an hour at room temperature. Gradually raise the temperature until it reaches 90 °C, stirring constantly until the gel form is reached. It's possible to see a gel-like substance forming on top of the solution in the beaker glass after 30 minutes of stirring at 90 °C, as shown in Figure (1 c). This is because of a high viscosity of solution and the fact that it is still on the magnetic stirrer and in the beaker glass at this point. A temperature decreases to room temperature after the solution turns to gel, the gel dries, and the hue changes to dark brown. An oven at 150°C for three hours can be used to dry and lower the gel's weight by placing the gel's weight in a glass beaker with a sensitive balance (1d). Dry gel began to convex in the beaker after 15 minutes after evaporating some of the substance and boosting the gel's temperature to (250°C), as depicted in figure (1 e). Following combustion, the dried gel becomes a fine powder that has a dark gray tint, indicating the commencement of high purity ferrite production, as shown in the photo (1f). The spinel was then calcined for three hours at temperatures of (650,750, and 850 C) to improve crystallization and homogenous action distribution, and then ground to produce $Zn_xMn_{1-x}Fe_2O_4$ ferrite Nano powders. Using the traditional ceramic method, titanium dioxide is mixed with zinc-manganese ferrite in different quantities at 500°C.

ISSN: 1343-4292
Volume 140, Issue 01, April, 2022

Figure (1): Photograph of (a) nitrates-citrate solution, (b) The solution after the Adding of ammonia, (c) dry gel, (d) Dry bulk temperature of 150℃, (e) Dry bulk temperature of 250℃ and (f) auto combustion and become Nano powder ferrite.

2.3 Characterization

(CuK) radiation (1.5418) was used to conduct XRD studies of Zn-Mn-Fe_2O_4. When employing step scan mode, the intensity data was taken in the range of (10^o-80^o) (XRD-6000). Zn-Mn- Fe_2O_4 generated samples were studied by XRD in the Nanotechnology and Advanced Materials, Baghdad-Iraq Nanotechnology Laboratory. A "(Tescan Mira3 FESEM-Czech)" in Iran-Mashhad has evaluated the morphology and particle size of Zn-Mn-Fe_2O_4 using FE-SEM. Fourier transformed infrared spectrum (FTIR) was employed in the study of the functional group and vibration modes, with a potassium bromide beam splitter and a mid IR TGC detector used to perform the polarized IR reflectance. The magnetic characteristics were examined utilizing an MPMS XL, Quantum Design SQUID magnetometer by VSM [15].

3. Result and Discussion

3.1 XRD patterns

The x-ray diffraction (XRD) exam carried out to investigate the crystal structure type and the crystalline size of prepared $Zn_xMn_{1-x}Fe_2O_4$ ferrite nanocomposites (x = 0.15) at different calcination temperatures (650, 750 and 850 ^oC) [16].

Figures 2 presents the XRD patterns of $Zn_xMn_{1-x}Fe_2O_4$ ferrite nanocomposites at the concentrations (x= 0.15) at different calcination temperatures (650, 750 and 850 ^oC), respectively. The detected characteristic peaks at zinc concentration (x = 0.15) revealed the formation of cubic spinel $Zn_xMn_{1-x}Fe_2O_4$ crystal structure with space group (Fd-3m no.227) (marked with red stars), corresponding with the cubic structure (JCPDS 98-017-0912), in addition to the same cubic $MnFe_2O_4$ crystal structure with space group (Ia-3 no. 206) as shown in figure 2 [17- 22]. The increase in the concentration of zinc metal led to an increase in the crystallization of the cubic $Zn_xMn_{1-x}Fe_2O_4$ ferrite nanocomposite phase and the obtained peaks became more clear and intense. The crystallite sizes (D) was determined by Scherrer's Equation [23- 25].

$$D\ (nm) = \frac{K\,\lambda}{\beta\ \mathrm{Cos}\ \theta} \qquad (4)$$

Where λ is the wavelength (0.15418), k is called shape factor (0.9), (CuK_α), θ is a diffraction angle, and β is full width at half maximum (FWHM) [26- 28]. The XRD measurements of ($Zn_{0.15}Mn_{0.85}Fe_2O_4$) nanocomposite at the temperature (650, 750 and 850 ^oC) respectively, as shown in table (1).

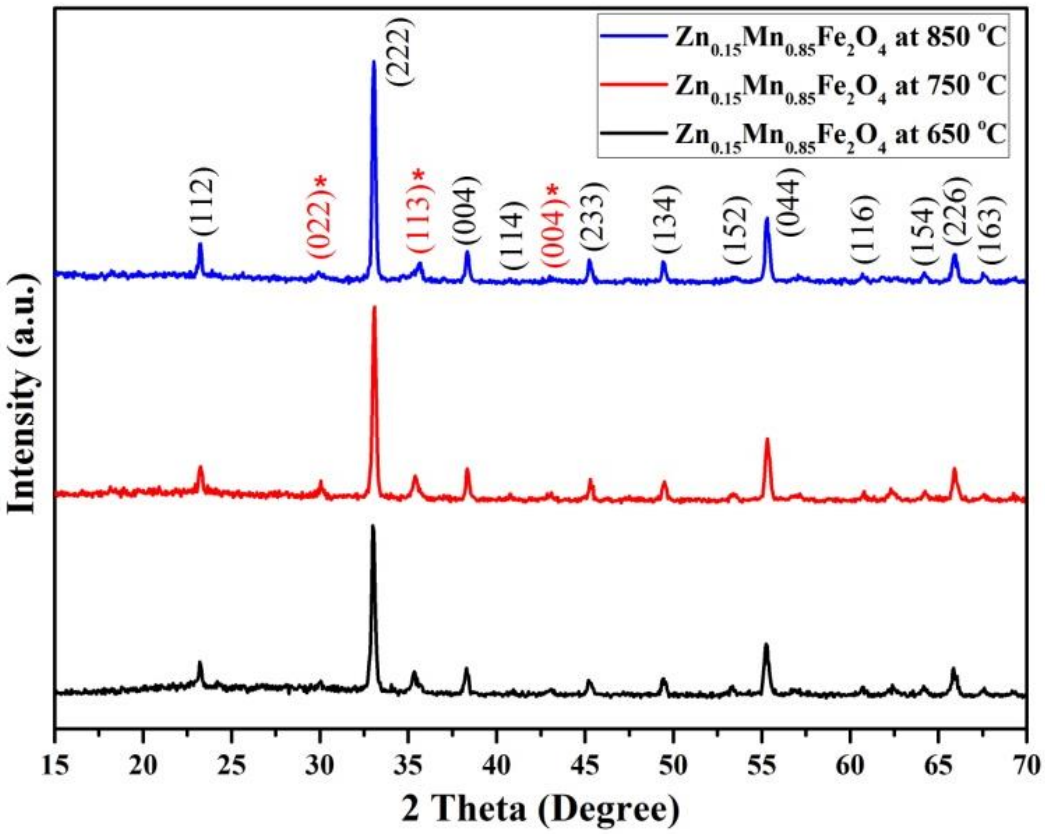

Figure (2): XRD patterns of $Zn_{0.15}Mn_{0.85}Fe_2O_4$ ferrite nanocomposites at different calcination temperatures (650, 750, 850 ˚C).

Table 1 XRD calculations of $Zn_xMn_{1-x}Fe_2O_4$ with different content of zinc metal (x=0.15) at different calcination temperatures.

Material	Temp. ºC	2Θ (deg) Practical	2Θ (deg) Standard	FWHM (deg)	Crystalline size (nm)	d_{hkl} (°A) Practical	d_{hkl} (°A) Standard	(hkl)
$Zn_{0.15}Mn_{0.85}Fe_2O_4$	650	35.40	35.24	0.4904	15.43	2.5354	2.5441	(113)
	750	35.40	35.24	0.4436	17.06	2.5352	2.5441	(113)
	850	35.29	35.24	0.4152	18.23	2.5387	2.5441	(113)

3.2 FE-SEM analysis

Tests on ZnxMn1-xFe_2O_4 showed that the particles had a spherical form and had a narrow variation of nanoparticle sizes, indicating that the particles were generated and had a porous structure. Particles of smaller size, such as spherical ones, have a persistent magnetic that results from their aggregation and clustering, therefore we perceive a homogeneous agglomeration of these particles. Figure (3) demonstrate the effects of increasing temperature on particle size in various forms, as shown in experiments performed using values of (x= 0.15) at temperatures of (650), (750), and (850 °C), respectively. The particles size and the shape of materials are 83 to 96 nm with cubic structure-like. The result of the particle size with the shape, as shown in table (2).

ISSN: 1343-4292
Volume 140, Issue 01, April, 2022

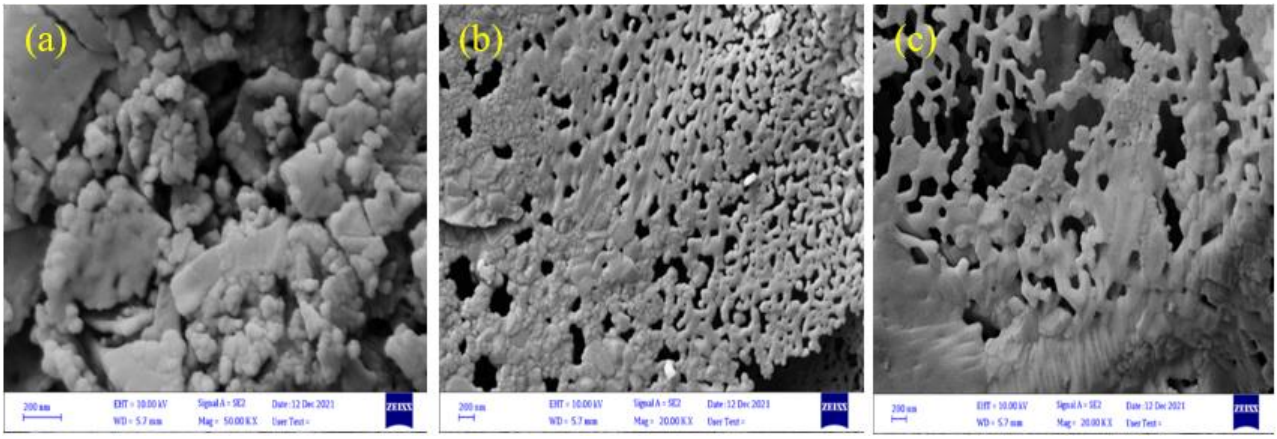

Figure (3): FE-SEM micrographs of $Zn_{0.15}Mn_{0.85}Fe_2O_4$ Nano ferrites for (a) calcined specimen at 650 ℃ (c) at 750 ℃ and (d) at 850 ˚C.

Table (2): FE-SEM measurements of $Zn_xMn_{1-x}Fe_2O_4$ with different content of zinc metal (x=0.15) at different calcination temperatures.

x	**Composition**	**Temp.˚*C***	**Particle size (nm) FESM**
0.15	$Zn_{0.15}Mn_{0.85}Fe_2O_4$	650	**83.86**
		750	**89.22**
		850	**96.54**

3.3 FT-IR spectrum

The Functional Group Analysis, the absorpption peak strong, and the compounds were determining by fourier transform infrared (FT-IR) spectrum of prepared $Zn_xMn_{1-x}Fe_2O_4$ ferrite nanocomposites (x = 0.15) at different calcination temperatures (650, 750 and 850 ^oC), respectively synthesized by sol-gel method.

The FT-IR spectrum of $Zn_xMn_{1-x}Fe_2O_4$ ferrite nanocomposites at the concentrations (x= 0.15), as shown in figure (4). Analyses of 567-667, 1640 and 3420 cm-1 show that there are multiple distinct peaks. Mn-O, Fe-O, and Zn-O bonds' vibrations in octahedral and tetrahedral sites. The FTIR data of the ferrite systems, which have a general spectrum at a frequency of roughly 400-600 cm^{-1}, agrees well with these findings [29]. Another study found that the C=C bending was a significant contributor to the vibration at 2338, and 2934 cm^{-1} [30]. The FT-IR measurements of ($Zn_{0.15}Mn_{0.85}Fe_2O_4$) nanocomposite at the temperature (650, 750 and 850 ^oC) respectively, as shown in table (3).

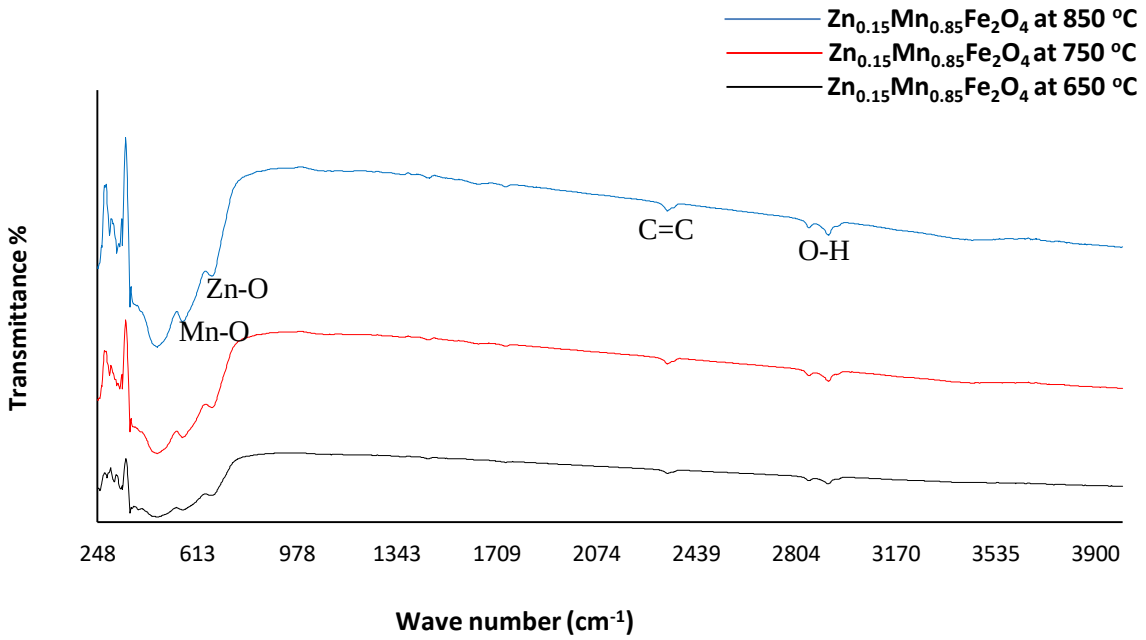

Figure (4): FT-IR spectrum of $Zn_{0.15}Mn_{0.85}Fe_2O_4$ ferrite nanocomposite at different calcination temperatures (650, 750, and 850 °C) by sol-gel method.

Table (3): FT-IR measurements of $Zn_xMn_{1-x}Fe_2O_4$ with different content of zinc metal (x=0.15) at different calcination temperatures.

Material	Temp. °C	The strong band (cm^{-1})	Compounds types	Absorption regions
$Zn_{0.15}Mn_{0.85}Fe_2O_4$	650	465	Fe-O	fingerprint region
	750	567	Mn-O	fingerprint region
	850	667	Zn-O	fingerprint region

3.4 VSM analysis

Nanocomposite $Zn_xMn_{1-x}Fe_2O_4$ ferrite nanocomposites (x = 0.15) were analyzed by VSM to determine the magnetization versus field M (H) at (650, 750, and 850 °C). Figures (5) show VSM analysis of pure $MnFe_2O_4$ ferrite nanocomposites and doped with different concentrations of zinc metal $Zn_xMn_{1-x}Fe_2O_4$ (x= 0.15) prepared by using sol-gel method. With maximum applied magnetic field, the M-H hysteresis loops of the (27 to 30) nm of $Zn_xMn_{1-x}Fe_2O_4$ nanocomposite revealed typical superparamagnetic nature, with minor interactions between the particles, as demonstrated by the negligible coercivity of the nanocomposite. The superparamagnetic matrix had a modest volume proportion of ferromagnetic phases. Nanoparticle size increased all metrics, such as the maximum magnetization (M_{max}), coercivity (Hc), and the residual ratio M_r/M_{max}, which indicated an increase in inter-particle interactions. Exchange and dipolar contacts are the two forms of magnetic nanoparticle interactions. Thermal energy dominates over exchange energy, reducing M_{max}, Hc, and M_r/M_{max} when the particle size is small enough, as shown in figure (5). In order to test the impact of sintering temperature on Mn–Zn ferrite, the composition $Zn_{0.15}Mn_{0.85}Fe_2O_4$ is utilized [31]. The VSM measurements of ($Zn_{0.15}Mn_{0.85}Fe_2O_4$) nanocomposite at the temperature (650, 750 and 850 °C) respectively, as shown in table (4) [32- 34].

ISSN: 1343-4292
Volume 140, Issue 01, April, 2022

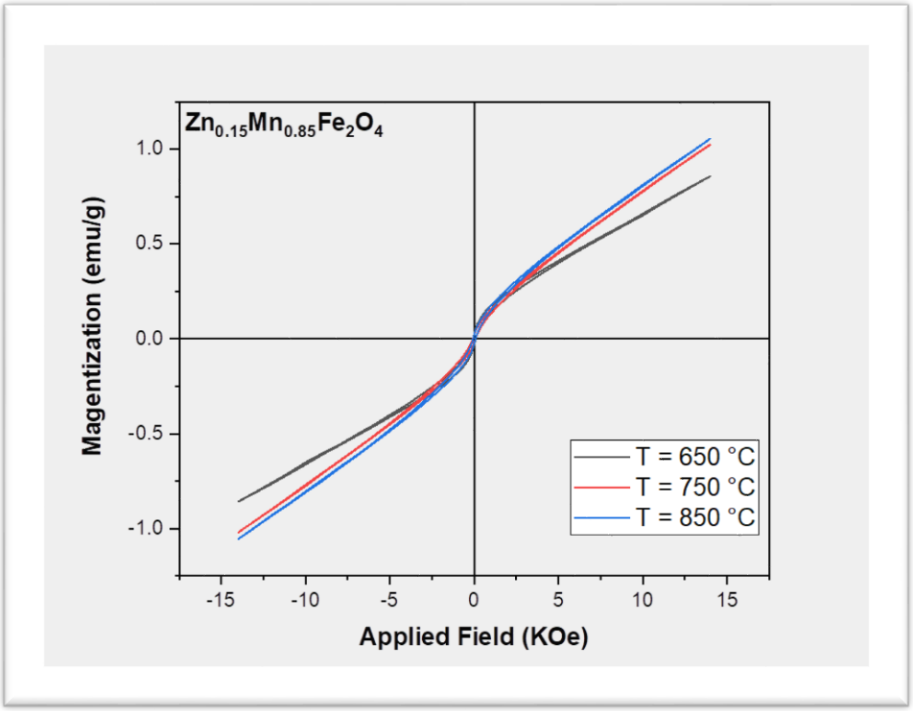

Figure (5): VSM analysis of $Zn_{0.15}Mn_{0.85}Fe_2O_4$ ferrite nanocomposites at different calcination temperatures (650, 750, and 850 ˚C).

Table (2): VSM measurements of $Zn_{0.15}Mn_{0.85}Fe_2O_4$ nanocomposite with different content of zinc metal at different calcination temperatures (650, 750, and 860) ºC.

Temp	H_c (Oe)	M_r (emu/g)	M_s (emu/g)	M_r/M_s	n_B (μ_B)	K (emu.Oe.g^{-1})
650	17.5	0.022	12.57	0.0018	0.057	29
750	16.3	0.015	1.52	0.0095	0.055	26
850	57	0.030	1.37	0.0220	0.049	81

4. Conclusions

In this study, Mn-Zn-Fe_2O_4 nanocomposite was successfully synthesized by sol–gel method at 650, 750, and 850 ºC (X=0.15). XRD results confirm pure cubic spinel crystalline structure for the sample. The average crystallite size was calculated by Debye-Scherrer formula. An examination into the possibility of producing the Mn-Zn-ferrites (NPs) by sol-gel as prospective structure-tunable nanomaterials is described in this report. X-ray diffraction (XRD), field emission-scanning electron microscopy (FE-SEM), Fourier-transform infrared (FTIR) spectroscopy and Vibrating Sample Magnetometer (VSM) analysis were used to characterize the structural and magnetic properties of the Mn-Zn-ferrites by sol-gel. Sized between 15 and 18 nm, the cubes in the XRD images reveal that the particles have a cubic structure. FE-SEM scans showed the synthesized the Mn-Zn-ferrites had a nanoparticle-like structure with a particle size of 27.77, to 72.04 nm. The strong FT-IR absorption peakset al at 400 and 500 cm^{-1} represented an Fe-O, Mn-O, and Zn-O vibration band for the Mn-Zn-ferrites, respectively. Results from the VSM showed that the magnetic nature of materials changed significantly from pristine as magnetization increased and coercivity decreased with Mn-Zn-ferrites nanoparticles. Finally, an optimized magnetic parameter value (Ms =0.80 emu/g and Hc =75 Oe) at (850) ºC was obtained from the results.

5. References

[1] X. Hou, J. Feng, X. Liu, Y. Ren, Z. Fan, and M. Zhang, "Magnetic and high rate adsorption properties of porous Mn(1-x)Zn(x)Fe2O4 ( ) adsorbents," J. Colloid Interface Sci., vol. 353, pp. 524–9, Jan 15, 2011.

[16] A. C Yang, C. N. , J. M. Greneche, Y. Chen, S. D. Yoon, K. Hsu, C. Vittoria, and V. G. Harris, "Large tunability of Néel temperature by growth-rate-induced cation inversion in Mn-ferrite nanoparticles," Elect. Comput. Eng. Faculty Pub., 2009.

[17] P. P. M. El Guendouzi and B. Gillot, "Oxidation mechanism of manganese-zinc ferrites in relation with cationic distribution below 700 ," Mater. Chem. Phys., vol. 25, pp. 429–436, 1990.

[18] P. Hu, H.-B. Yang, D.-A. Pan, H. Wang, J.-J. Tian, and S.-G. Zhang et al., "Heat treatment effects on microstructure and magnetic properties of Mn-Zn ferrite powders," J. Magn. Magn. Mater., vol. 322, pp. 173–177, 2010.

[19] Y. A. K. S. P. Gubin, G. B. Khomutov, and G. Y. Yurkov, "Magnetic nanoparticles: Preparation, structure and properties," Russian Chem. Rev., vol. 74, pp. 489–520, 2005.

[20] A. H. Morrish, The Physical Principles Of Magnetism. New York, NY, USA: Wiley, 1965. [7] M. H. Mahmoud, H. H. Hamdeh, J. C. Ho, M. J. O'Shea, and J. C. Walker, "Mössbauer studies of manganese ferrite fine particles processed by ball-milling," J. Magn. Magn. Mater., vol. 220, pp. 139–146, 10, 2000.

[21] B. Z. C. Liu, A. J. Rondinone, and Z. J. Zhang, "Reverse Micelle synthesis and characterization of superparamagnetic MnFe2O4 Spinel ferrite nanocrystallites," J. Phys. Chem. B, vol. 104, p. 1141, 2000.

[22] R. D. K. Misra, S. Gubbala, A. Kale, and W. F. Egelhoff, "A comparison of the magnetic characteristics of nanocrystalline nickel, zinc, manganese ferrites synthesized by reverse micelle technique," Mater. Sci. Eng.: B, vol. 111, pp. 164–174, 2004.

[23] S. Dasgupta, J. Das, J. Eckert, and I. Manna, "Influence of environment and grain size on magnetic properties of nanocrystalline Mn-Zn ferrite," J. Magn. Magn. Mater., vol. 306, pp. 9–15, 2006.

[24] R. Arulmurugan, B. Jeyadevan, G. Vaidyanathan, and S. Sendhilnathan, "Effect of zinc substitution on Co-Zn and Mn-Zn ferrite nanoparticles prepared by co-precipitation," J. Magn. Magn. Mater., vol. 288, pp. 470–477, 2005.

[25] J. Li, H. Yuan, G. Li, Y. Liu, and J. Leng, "Cation distribution dependence of magnetic properties of sol-gel prepared MnFe2O4 spinel ferrite nanoparticles," J. Magn. Magn. Mater., vol. 322, pp. 3396–3400, 2010.

[26] D. G. B Bhattacharjee, K. Iakoubovskii, A. Stesmans, and S. Chaudhuri, "Synthesis and characterization of sol-gel derived ZnS: Mn2+ nanocrystallites embedded in a silica matrix," Bull. Mater. Sci., vol. 25, pp. 175–180, Jun. 2002. [27] A. K. M. A. Hossain, S. T. Mahmud, M. Seki, T. Kawai, and H. Tabata, "Structural, electrical transport, magnetic properties of Ni1-xZnxFe2O4," J. Magn. Magn. Mater., vol. 312, pp. 210–219, 5, 2007.

[28] S. Matussin, M. H. Harunsani, A. L. Tan, M. Mansoob Khan, Plant-Extract-Mediated SnO2

Nanoparticles: Synthesis and Applications, ACS Sustainable Chem. Eng. 2020, 8, 8, 3040-3054.

[29] Suharyadi, E., Setiadi, E. A., Shabrina, N., Kato, T., & Iwata, S. (2014). Magnetic properties and microstructures of polyethylene glycol (PEG)-coated cobalt ferrite (CoFe2O4) nanoparticles synthesized by coprecipitation method. In Advanced Materials Research (Vol. 896, pp. 126-133). Trans Tech Publications Ltd.

[30] Manohar, A., Krishnamoorthi, C., Pavithra, C., & Thota, N. (2021). Magnetic hyperthermia and photocatalytic properties of MnFe2O4 nanoparticles synthesized by solvothermal reflux method. Journal of Superconductivity and Novel Magnetism, 34(1), 251-259.

[31] Köseoğlu, Y., Baykal, A., Toprak, M. S., Gözüak, F., Başaran, A. C., & Aktaş, B. (2008). Synthesis and characterization of ZnFe2O4 magnetic nanoparticles via a PEG-assisted route. Journal of Alloys and Compounds, 462(1-2), 209-213.

[32] Abid, M. A., & Kadhim, D. A. (2021). Synthesis of iron oxide nanoparticles by mixing chilli with rust iron extract to examine antibacterial activity. Materials Technology, 1-10.

[33] Abid, M. A., Kadhim, D. A., & Aziz, W. J. (2020). Iron oxide nanoparticle synthesis using trigonella and tomato extracts and their antibacterial activity. Materials Technology, 1-8.

[34] Kadhim, D. A., Abid, M. A., Abdulghany, Z. S., Yahya Alhatem, J., Kadhim, S. A., Aziz, W. J., & Al-Marjani, M. F. (2022). Iron oxide nanoparticles synthesized using plant (Beta vulgaris and Punica granatum) extracts for a breast cancer cell line (MCF-7) cytotoxic assay. Materials Technology, 1-9.